Rapid Communications   Editors' Suggestion

Emergent Fermi surface in a many-body non-Hermitian fermionic chain

Sen Mu, Ching Hua Lee ⬤,* Linhu Li ⬤, and Jiangbin Gong†
Department of Physics, National University of Singapore, Singapore 117542

Quantum degeneracy pressure (QDP) underscores the stability of matter and is arguably the most ubiquitous many-body effect. The associated Fermi surface (FS) has broad implications for physical phenomena, ranging from electromagnetic responses to entanglement entropy (EE) area law violations. Given recent fruitful studies in condensed-matter physics under effectively non-Hermitian descriptions, it becomes urgent to study how QDP and many-body interactions interplay with non-Hermitian effects. Through a prototypical critical one-dimensional fermionic lattice with asymmetric gain/loss, a real space FS is shown to naturally emerge, in addition to any existing momentum space FS. We carefully characterize such real space FS with the EE, by a renormalized temperature that encapsulates the interplay of thermal excitations and non-Hermiticity. Nearest-neighbor repulsion is also found to induce a competing charge density wave (CDW) that may erode the real space FS. The underlying physics surrounding criticality and localization is further analyzed with complex flux spectral flows. Our findings can be experimentally demonstrated with ultracold fermions in a suitably designed optical lattice.

In a wide variety of systems such as quantum Hall liquids, superconductors, and neutron stars, it is the emergent many-body effects, rather than the single-particle behavior, that give rise to their respective signature properties. Arguably quantum degeneracy pressure (QDP) represents the most ubiquitous many-body effect, where the Pauli exclusion principle underscores both the rigidity of everyday-life solids [1–3] and the stability of neutron stars [4]. A primary consequence of QDP is the formation of a Fermi surface (FS), which bounds a sea of impenetrable fermions in optimal energetic configuration. Dictating the available quasiparticle excitations and semiclassical contours, the shape of the FS crucially controls transport, magnetization, and optical properties [5–14]. As an extended critical region, a FS also violates the celebrated area law for entanglement entropy (EE), whose deep relation with many-body couplings have spurred the study of holographic duality [15–26].

Non-Hermitian descriptions of condensed-matter systems [27–63] have provided an effective and fruitful framework to account for inelastic collisions [28], disorder effects [29–31,42,43,63], and system-environment couplings [32–35]. This research avenue has extended the domain of condensed-matter physics with inspiring insights. It is therefore necessary and urgent to study the implications of non-Hermiticity for QDP. In particular, nonreciprocal hopping in a lattice system defines a preferred pumping direction, thereby causing all eigenstates at the single-particle level to accumulate at the boundaries. However, this non-Hermitian phenomenon, coined the non-Hermitian skin effect [48–59,61],

cannot possibly persist in the presence of QDP and many-body interactions, which will at the very least prohibit multiple occupancy at the boundaries.

In this work, we show that nonreciprocal pumping yields an eigenstate spatial profile that not only resembles a Fermi surface in real space [64], but also behaves as a genuine FS at the level of entanglement entropy, characterized by a renormalized temperature depending on both physical temperature and hopping asymmetry. Though spatial particle accumulation is not physically identical with the Fermi sea condensation in energy space, universal scaling behaviors of EE is a testimony to the fact that this emergent FS corresponds to a bona fide FS. Furthermore, we observe the erosion of the emergent FS by the charge-density wave (CDW) arising from the nearest-neighbor (NN) repulsion. Finally, we visualize these interplays in terms of spectral flows, and suggest a cold-atom setup for future experimental demonstration.

Interacting fermions with asymmetric gain/loss. We consider a minimal model that captures the interplay between asymmetric non-Hermitian gain/loss and two types of many-body effects: (i) fermionic QDP and (ii) NN repulsion. As illustrated in Fig. 1(a), it consists of spin-polarized repulsive fermions hopping along a chain of length L with open boundary conditions (OBCs):

$$H = \sum_{x=1}^{L-1} \{J(e^{\alpha} c_x^{\dagger} c_{x+1} + e^{-\alpha} c_{x+1}^{\dagger} c_x) + U n_x n_{x+1}\}, \quad (1)$$

where $c_x^{\dagger}/c_x$ is the fermion creation/annihilation operator at site x and $n_x = c_x^{\dagger} c_x$ is the corresponding fermion number operator. Two fermions are forbidden from occupying the same site, and will incur an energy penalty of $U > 0$ if they occupy adjacent sites. The nonreciprocal left/right hoppings $Je^{\pm\alpha}$ can be understood as asymmetric gain/loss and are
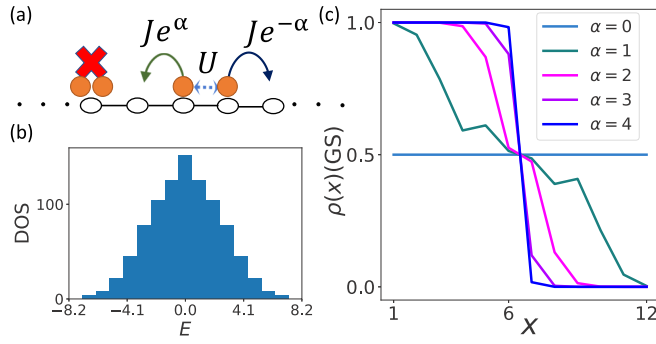
*phylch@nus.edu.sg
†phygj@nus.edu.sg

FIG. 1. (a) Our fermionic chain Eq. (1) with asymmetric gain/loss $Je^{\pm\alpha}$ and NN interactions U. (b) Its OBC density of states (DOS) at $U = 0$, corresponding to a real gapless spectrum. (c) Spatial density of the GS at $U = 0$ and half filling $L = 2n = 12$, which reveals a real space FS that becomes sharper with increasing α asymmetry.

within reach of experiments [65–68]. Unless otherwise stated, we shall assume half filling (presence of $n = L/2$ fermions).

The OBC spectrum of this simple ansatz system is always real and gapless [Fig. 1(b)], as seen through the spatially inhomogeneous similarity transform $c_x^\dagger \to c_x^\dagger e^{x\alpha}$, which eliminates the $e^{\pm\alpha}$ factors in Eq. (1) and keeps n_i invariant [69]. As such, familiar concepts like the ground state (GS) and energy gaps remain applicable. Since the spectrum is agnostic to the non-Hermitian asymmetry α, the interplay between many-body effects and non-Hermiticity is only manifested at the *eigenstate* level. Henceforth we focus on the right eigenstates $|\psi^R\rangle$ defined by $H|\psi^R\rangle = \varepsilon|\psi^R\rangle$ with normalization condition $|\langle\psi^R|\psi^R\rangle|^2 = 1$, except when studying broader implications on bulk-boundary spectral correspondences.

Emergent real space Fermi surface. Demarcating the occupied Hilbert space boundary, a FS plays a dual role to the entanglement cut and allows the EE to be expressed in a position-momentum symmetric manner [70–72]. As such, a real space FS can coexist on an equal footing with an ordinary momentum space FS.

Here we show how a real space FS emerges naturally from the interplay of non-Hermiticity and QDP. Consider first the case without NN repulsion ($U = 0$). At the single-particle level, $H|_{U=0}$ possesses non-Bloch eigenstates $\psi_j(x) = \mathcal{N}_j e^{-x\alpha} \sin\frac{\pi j x}{L+1}$ with corresponding eigenenergies $\varepsilon_j = 2J\cos\frac{\pi j}{L+1}$ and normalization constants $\mathcal{N}_j$ [73]. For $\alpha > 0$, the eigenstates are all exponentially localized at the left boundary ($x = 1$) with localization length α^{-1}, as implied by the above-mentioned similarity transformation. Physically, they also represent the steady-state solutions of a biased random walk on a bounded one-dimensional (1D) chain.

Multiple fermions, however, will not be allowed to all localize at $x = 1$ due to QDP. We characterize the spatial density of an n-fermion state $\psi_\mu^R(x_1, \ldots, x_n)$ by $\rho_\mu(x) = \langle\psi_\mu^R|n_x|\psi_\mu^R\rangle$, and define the thermal-weighted density $\rho(x) = \binom{N}{n}^{-1}\sum_\mu e^{-\beta E_\mu}\rho_\mu(x)$ with temperature β^{-1}, where E_μ is the energy of ψ_μ. For $\beta \to \infty$, we obtain the GS density $\rho(x)$(GS).

From Fig. 1(c), $\rho(x)$(GS) is seen to be spatially uniform for reciprocal hopping ($\alpha = 0$). As α increases, we observe

a competition between asymmetric hoppings $e^{\pm\alpha}$ and QDP: While even a tiny α has the propensity to localize each fermion towards the left boundary, the QDP forces all the n fermions to forbid another from occupying the same site. As such, $\rho(x)$(GS) is symmetric about the n and $(n + 1)$th site, with the profile controlled by the exponential tail of a single-fermion eigenstate. In the extremely asymmetric limit of $|\alpha| \to \infty$, hoppings become unidirectional, and the density profile becomes a jump discontinuity. Note that this nontrivial compromise of QDP and asymmetric gain/loss only applies to fermions, since multiple bosons will be allowed to condense macroscopically at one boundary, just like isolated bosons.

From Fig. 1(c), $\rho(x)$(GS) very closely resembles a Fermi-Dirac spatial profile of the form $\rho_{FD}(x) = (1 + e^{\Lambda(x-n-1/2)})^{-1}$, with $\Lambda \sim 4\alpha$ rigorously derivable from the Slater determinant [73]. Attractive as this identification looks, Λ *cannot* represent an effective inverse temperature because it is conjugate to position, not energy. To transcend this subtlety and determine the exact sense in which we have an emergent real space FS, a universal recourse is the entanglement entropy, whose scaling behavior reveals both the temperature and FS properties. Conformally transforming standard results [16,74], the EE $S_{ent,\beta}$ of a finite critical half-filled 1D system scales like

$$S_{ent,\beta} \sim \frac{c}{6}\ln\left[\frac{\beta}{\pi}\sinh\frac{\pi L_A}{\beta}\right] + \text{const}, \quad (2)$$

where β is the inverse temperature, L_A is the length of the left subsystem, and $c = 1$ is the central charge for our fermionic model. Its logarithmic form violates the area law of EE scaling, which states that the EE of a gapped 1D system should plateau beyond a sufficiently large system size. In the following, we shall also investigate how this violation is further modified by non-Hermiticity α.

In this work, we shall define the density matrix with respect to the right eigenvectors to compute EE, because we are interested in the eigenstates themselves, rather than computing probability-conserving expectation values of observables [75,76]. From $[\rho^{RR}]_{\mu\nu} = |\psi_\mu^R\rangle\langle\psi_\nu^R|$, we can trace out degrees of freedom other than those in the left subsystem A and define a reduced density matrix $\rho_A^{RR} = \text{Tr}_{A^c}|\psi^R\rangle\langle\psi^R| = \sum_r \lambda_r^2|\psi_{r,A}^R\rangle\langle\psi_{r,A}^R|$, where $|\psi^R\rangle = \sum_r \lambda_r|\psi_{r,A}^R\rangle \otimes |\psi_{r,A^c}^R\rangle$ is the Schmidt decomposition of a representative $|\psi^R\rangle$ and A^c is the right subsystem, i.e., the complement of A. The entanglement entropy with respect to the entanglement cut separating A and A^c is the corresponding von Neumann entropy,

$$\begin{aligned} S_{ent,A} &= -\text{Tr}[\rho_A^{RR}\ln\rho_A^{RR}] \\ &= -\sum_r [\lambda_r\ln\lambda_r + (1 - \lambda_r)\ln(1 - \lambda_r)], \quad (3) \end{aligned}$$

where λ_r is the eigenvalue of ρ_A^{RR}. EE is a good measure of entanglement for a pure quantum state, while it is not for a mixed state since the von Neumann entropy mixes quantum and classical correlations [74].

From Fig. 2(a), S_{ent} behaves very differently across the regimes of weak and strong α, demarcated at $\alpha_0 = 0.8\ln(L - 1) \approx 2$ [73] for $L = 12$. In the weak α regime, which is further elaborated in Fig. 2(c), S_{ent} varies strongly with both α and inverse temperature β, suggestive of their strong interplay.
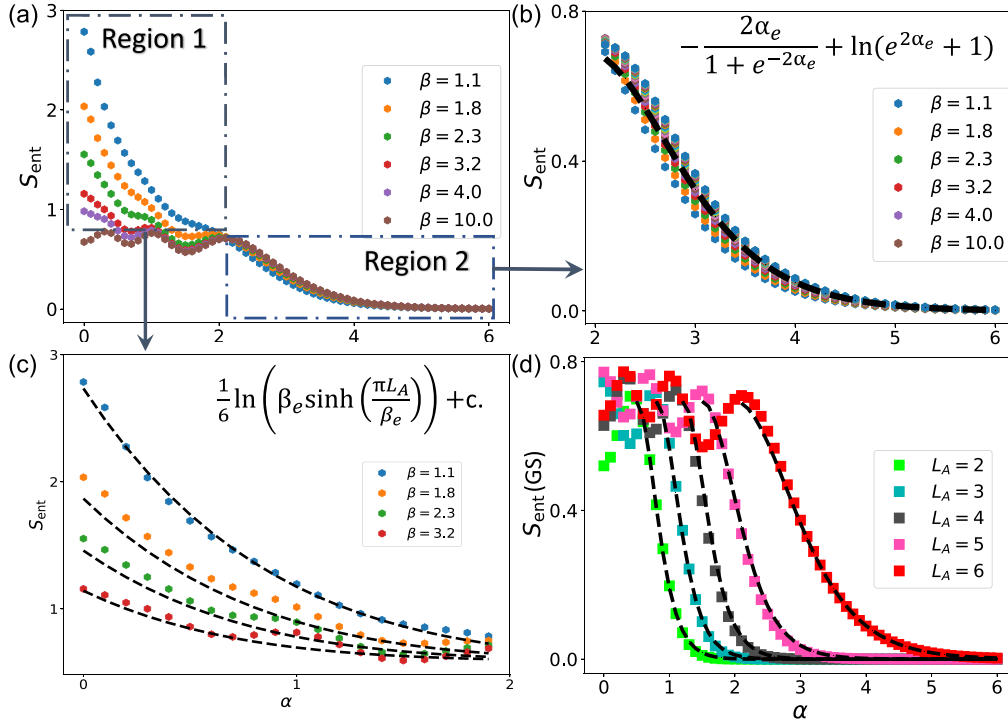
FIG. 2. EE behavior of the left subsystem A giving rise to renormalized temperature and hopping asymmetry. (a) OBC EE vs α at different inverse physical temperatures β with $L = 2L_A = 12$ at half filling. The β-independent $\alpha > \alpha_0$ (Region 2) and logarithmically scaling $\alpha < \alpha_0$ (Region 1) are detailed in (b) and (c), respectively. (b) Large α regime fitted to Eq. (4) with renormalized asymmetry $\alpha_e = \eta(\alpha - \alpha_0)$, where $\alpha_0 = 2, \eta = 1$. (c) Small α regime fitted to S_{ent,β_e} from Eq. (2) with renormalized inverse temperature $\beta_e = e^{0.9\alpha}\beta$. (d) OBC EE vs α at zero temperature for different subsystem lengths L_A and $L = 12$ at half filling. Equation (4) still fits excellently, with $\alpha_0 = \{0.5, 0.8, 1.2, 1.5, 2.0\}$ and $\eta = \{3.0, 2.7, 2.5, 1.7, 1.0\}$ for $L_A = \{2, 3, 4, 5, 6\}$.

In the strong α regime [Fig. 2(b)], however, S_{ent} shows little dependence on β, suggesting that sufficiently strong hopping asymmetry $e^{\pm\alpha}$ generates a robust real space FS that dominates any smudging effect from the original thermal ensemble.

Renormalized temperature and gain/loss asymmetry. Interestingly, the effect of the α in the weak asymmetry regime $\alpha < \alpha_0$ at finite temperature can be understood as a *renormalization* of the effective inverse temperature [77]. Intuitively, asymmetric gain/loss pushes all fermions towards one side, decreasing their configurational freedom and hence increasing the cost of "'excitations." At the level of EE, this reduction of freedom reduces the entanglement, mirroring the entanglement drop with decreased thermal excitations. This is substantiated by the fitted curves in Fig. 2(c), where the EE for $0 < \alpha < \alpha_0$ is shown to agree very well at finite temperature with its *Hermitian* ($\alpha = 0$) expression Eq. (2), but at a renormalized inverse temperature $\beta_e = e^{0.9\alpha}\beta$ for $L_A = L/2 = 12$.

As explained in the Supplemental Material [73], the renormalized temperature generically follows the form $\beta_e = e^{c(L)\alpha}\beta$, where $c(L)$ has a rather weak dependence on L and saturates to a constant in the limit of $L \to \infty$. For practical size in feasible calculations such as ours here, $c(L) \approx 0.9$. This observed trend of β_e indicates that nonreciprocal pumping is exponentially effective in reducing the available degrees of freedom. Furthermore, substituting β_e into Eq. (2), we

obtain an EE expression that severely violates the area law with an exotic temperature dependence.

In the strong asymmetry regime of $\alpha > \alpha_0$, the EE becomes almost independent on the physical temperature β^{-1}, indicating that the EE is dominated by the sharp real space FS. This can be further understood through a two-qubit model, where it is the asymmetry parameter α that becomes renormalized instead. Due to the sharp FS, we can approximate a generic state when $\alpha \geqslant \alpha_0$ by $|\psi\rangle \propto e^{\alpha_e/2}|1_A 0_{\bar{A}}\rangle + e^{-\alpha_e/2}|0_A 1_{\bar{A}}\rangle$, where the states $|1_A 0_{\bar{A}}\rangle$ and $|0_A 1_{\bar{A}}\rangle$ can be understood as $|11\ldots11\rangle_A|00\ldots00\rangle_{\bar{A}}$ and $|11\ldots10\rangle_A|10\ldots00\rangle_{\bar{A}}$, respectively, with the last digit in A being the occupation number of the nth site and the first in $\bar{A}$ the $(n+1)$th site, and $A, \bar{A}$ are the left and right subsystems, respectively, demarcated by an entanglement cut. Taking a partial trace over the $\bar{A}$ qubit in the density matrix $\rho = |\psi\rangle\langle\psi|$, we obtain the reduced density matrix $\rho_A = e^{2\alpha_e}/(1+e^{2\alpha_e})|0_A\rangle\langle0_A| + 1/(1+e^{2\alpha_e})|1_A\rangle\langle1_A|$, which possesses the EE

$$S_{\text{ent},A} = -\frac{2\alpha_e}{1+e^{-2\alpha_e}} + \ln(e^{2\alpha_e}+1), \quad (4)$$

which from Fig. 2(b) agrees very well with the actual EE of our model Eq. (1) when $\alpha > \alpha_0$, with the renormalized α simply given by $\alpha_e = \alpha - \alpha_0$. This validates our two-qubit caricature in the $\alpha > \alpha_0$ regime, below which thermal excitations are sufficiently strong to break down this two-level picture and produce EE beyond $\ln 2 \approx 0.69$.
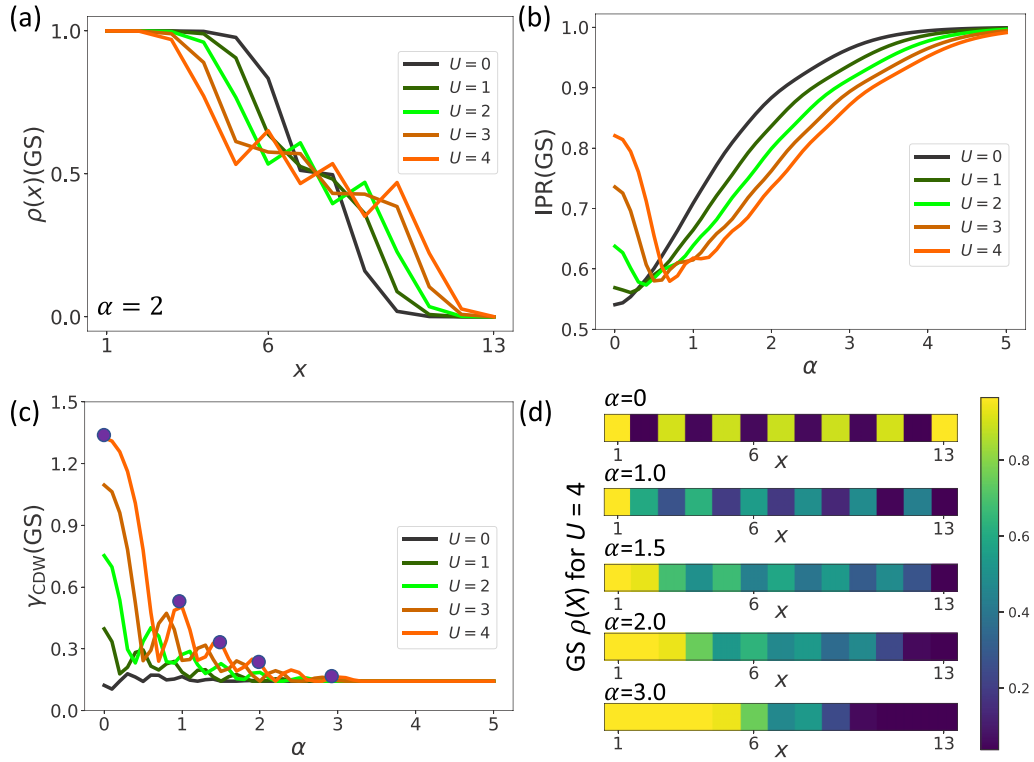
FIG. 3. NN interaction U which induces CDW interplay with α, all with $n = 7$ and $L = 13$. (a) Spatial GS density, with FS destabilized by increasing U. (b), (c) IPR/γ_{CDW} of the GS vs α, both of which are nonmonotonic with α. (d) GS spatial profiles at $U = 4$ and various α as indicated by the purple dots in (c). As α increases, the CDW gives way to the FS, with the localization (IPR) minimized at an intermediate stage.

At zero temperature, our two-qubit model remains fully applicable even when the entanglement cut does not coincide with the real space FS, i.e., $L_A \neq n$, where $n = L/2$ in our case for half filling. Shown in Fig. 2(d) are excellent fits of the EE S_{ent} with Eq. (4) for $L_A = 2$ to 6 ($n = 6$), with details of α_e given in the caption. For sufficiently large α, S_{ent} drops sharply when the emergent real space FS is not aligned with the entanglement cut, implying that the FS harbors most of the entanglement.

Competing CDW and asymmetric gain/loss. We now turn on the NN repulsion U and study how it can destabilize the emergent FS. Like QDP, nonzero $U > 0$ also serves to counteract boundary mode accumulation through repulsion. Indeed, as portrayed by Fig. 3(a), increasing U smooths out the FS in a way naively reminiscent of decreasing the α asymmetry.

A closer examination of the individual eigenstate profiles reveals striking differences between QDP, which acts relentlessly on all fermions, and U repulsion, which only assigns finite energy penalties. We consider the inverse participation ratio (IPR) [78] defined as IPR $(\mu) = \frac{1}{n} \sum_{x=1}^{L} |\langle \psi_\mu^R | n_x | \psi_\mu^R \rangle|^2$. IPR (μ) hence reveals the real space locality of the μth right eigenstate ψ_μ^R: IPR $(\mu) = n/L$ or 1 in the extreme cases where ψ_μ^R is spatially uniform or each fermion is localized on one site, respectively. Focusing on the GS ($\mu = $ GS) which is minimally penalized by U, we observe an enigmatic trend in Fig. 3(b) where the IPR can vary nonmonotonically with α. In the $U = 0$ limit, the IPR simply increases monotonically

with α to its maximal value as the FS becomes sharper. But with nonzero NN repulsion U, the IPR actually dips before rising again, signifying a competing delocalizing influence.

Intuitively, the NN repulsion can favor CDWs because it repels adjacent fermions but allows them to accumulate freely as next NNs. To check if this intuition corroborates with the nonmonotonic IPR behavior, we compute the CDW imbalance parameter $\gamma_{\text{CDW}}(\mu) = \frac{2}{L} \sum_{x=1}^{L-1} |\rho_\mu(x+1) - \rho_\mu(x)|$ for $\mu = $ GS, which ranges from 0 to 2 depending on how closely the GS assumes a ferromagnetic or antiferromagnetic spatial density profile. From Fig. 3(c), it is evident that around the dip in IPR, the GS γ_{CDW} is indeed small even for moderately strong U. To completely interrogate this CDW behavior, we examine the density profiles of the $U = 4$ case at various α [Fig. 3(d)]. Indeed, the large IPR at small and large α are due to different reasons, namely, CDW and FS localization, respectively.

Spectral analysis of interplay. Ultimately, the real space FS is a consequence of fermion accumulation under OBCs, but not periodic BCs (PBCs). To understand the OBC accumulation more deeply at the level of the entire spectrum, we interpolate between OBC and PBC by adiabatically turning on the hoppings $Je^{\pm\alpha}$ and repulsion U between the first and the last sites from 0 to 100%. In general, PBC and OBC spectra and their respective eigenstate profiles can be drastically different. A longer OBC-PBC spectral flow trajectory implies stronger spatial accumulation [73], as shown
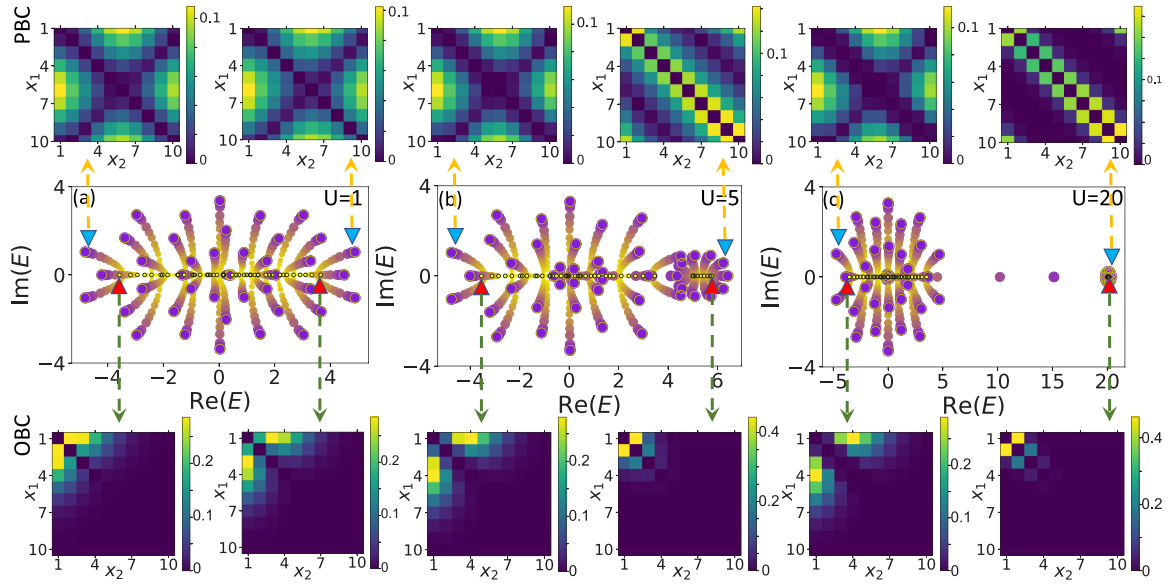
FIG. 4. (a)–(c) PBC vs OBC spectra for two fermions with various NN repulsion $U = 1, 5, 20$, and how the PBC-OBC spectral evolution reflects the interplay between NN repulsion and asymmetric gain/loss pumping. In the center row, the PBC/OBC eigenenergies are depicted by circled purple/small yellow dots. PBC and OBC spatial profiles of the lowest/highest Re(E) eigenstates, where U is effectively attractive/repulsive, is shown in the top and bottom rows. Shorter PBC-OBC evolution curves correspond to more similar spatial localization lengths. We used $\alpha = 1$ and $L = 10$ throughout.

in Fig. 4 for various NN repulsion strengths U between two fermions, where yellow-purple curves connecting the PBC eigenenergies (circled purple dots) collapse onto real OBC eigenenergies (small yellow dots). In the weakly repulsive $U = 1$ case, both PBC and OBC spectra are gapless (forming a single cluster), but larger U repulsions leads to the formation of a high-energy eigenenergy cluster (band), opening up a real OBC Mott gap.

The dispersion of this high-energy band, as well as the insulating gap width, can be partially understood from the OBC-PBC spectral flow. In the large $U = 20$ limit, a high-energy state experiences strong effective attraction instead of repulsion, and contains both fermions in adjacent sites. Since the localization property of this configuration is largely agnostic to boundary conditions, we expect its PBC to OBC trajectories to be very short (i.e., without an appreciable change in the inverse decay length of the eigenstates), with almost identical PBC and OBC eigenenergies and minute intraband dispersion. As U decreases, the PBC-OBC flow trajectories from the higher band necessarily get longer, and will eventually intersect with those from the lower band, as for $U = 5$. This gives a scenario where the OBC spectrum is gapped while the PBC spectrum is critical, which we also see is inevitable from the spectral flow analysis.

Proposed demonstration with cold atoms. Our emergent FS and competing CDW can be qualitatively realized in any fermionic lattice with effectively asymmetric hopping. Recently, it was realized that such nonreciprocal hopping can be effectively implemented (in a rotated representation) by introducing atom loss only [35,68,79]. This implementation is especially feasible in cold-atom systems trapped in optical lattices [80,81].

As an example, we propose a two-level setup $H = H_0 + H_{nH} + H_{int}$, with the Hermitian noninteracting part

$$H_0 = -\sum_j [it_q \hat{c}_{j,\uparrow}^\dagger \hat{c}_{j,\downarrow} + t_d(\hat{c}_{i,\uparrow}^\dagger \hat{c}_{j+1,\downarrow} - \hat{c}_{i,\uparrow}^\dagger \hat{c}_{j+1,\downarrow})$$
$$+ t_p(\hat{c}_{j,\uparrow}^\dagger \hat{c}_{j+1,\uparrow} - \hat{c}_{j,\downarrow}^\dagger \hat{c}_{j+1,\downarrow})] + \text{H.c.}, \quad (5)$$

on-site dissipation $H_{nH} = -ig\hat{c}_{i,\downarrow}^\dagger \hat{c}_{i,\downarrow}$ added to the pseudospin-down component, and $H_{int} = \sum_j \sum_{\sigma,\sigma'} U n_{j,\sigma} n_{j+1,\sigma'}$ ($\sigma = \uparrow, \downarrow$) being the NN interaction tunable by Feshbach resonance [80,81]. Note that H_0 has already been realized in a "two-tone" periodically shaken lattice with harmonic trapping frequencies of $(\omega_x, \omega_y, \omega_z) \approx 2\pi \times (41, 61, 130)$ Hz, where the pseudospin is simulated by two orbitals [82]. Non-Hermitian terms such as term H_{nH} may be synthesized by several mechanisms of considerable interest, namely, measurement backaction [83], measurement postselection [36,84,85], and on-resonance excitation [86–88], with Refs. [36] and [88] being two recent experimental realizations. The atomic density $\rho(x)$ can be experimentally resolved at atomic resolution [89–91] where measurement takes ~ 2 μs for each position to be imaged, and therefore experiments can indeed probe the interplay between the CDW and the FS localization. Clearly then, our proposal is already within reach of today's experimental techniques.

[1] F. J. Dyson and A. Lenard, Stability of matter. I, J. Math. Phys. **8**, 423 (1967).

[2] A. Lenard and F. J. Dyson, Stability of matter. II, J. Math. Phys. **9**, 698 (1968).

[3] F. J. Dyson, Ground-state energy of a finite system of charged particles, J. Math. Phys. **8**, 1538 (1967).

[4] J. R. Oppenheimer and G. M. Volkoff, On massive neutron cores, Phys. Rev. **55**, 374 (1939).

[5] Y. Zhao, H. Liu, C. Zhang, H. Wang, J. Wang, Z. Lin, Y. Xing, H. Lu, J. Liu, Y. Wang, S. M. Brombosz, Z. Xiao, S. Jia, X. C. Xie, and J. Wang, Anisotropic Fermi Surface and Quantum Limit Transport in High Mobility Three-Dimensional Dirac Semimetal Cd_3As_2, Phys. Rev. X **5**, 031037 (2015).

[6] Z. Zhu, X. Lin, J. Liu, B. Fauqué, Q. Tao, C. Yang, Y. Shi, and K. Behnia, Quantum Oscillations, Thermoelectric Coefficients, and the Fermi Surface of Semimetallic WTe_2, Phys. Rev. Lett. **114**, 176601 (2015).

[7] C. H. Lee, X. Zhang, and B. Guan, Negative differential resistance and characteristic nonlinear electromagnetic response of a topological insulator, Sci. Rep. **5**, 18008 (2015).

[8] T. Morimoto, S. Zhong, J. Orenstein, and J. E. Moore, Semiclassical theory of nonlinear magneto-optical responses with applications to topological Dirac/Weyl semimetals, Phys. Rev. B **94**, 245121 (2016).

[9] A. G. Grushin, J. W. F. Venderbos, A. Vishwanath, and R. Ilan, Inhomogeneous Weyl and Dirac Semimetals: Transport in Axial Magnetic Fields and Fermi Arc Surface States from Pseudo-Landau Levels, Phys. Rev. X **6**, 041046 (2016).

[10] P. J. W. Moll, N. L. Nair, T. Helm, A. C. Potter, I. Kimchi, A. Vishwanath, and J. G. Analytis, Transport evidence for Fermi-arc-mediated chirality transfer in the Dirac semimetal Cd_3As_2, Nature (London) **535**, 266 (2016).

[11] F. de Juan, A. G. Grushin, T. Morimoto, and J. E. Moore, Quantized circular photogalvanic effect in Weyl semimetals, Nat. Commun. **8**, 15995 (2017).

[12] K. Hamamoto, M. Ezawa, K. W. Kim, T. Morimoto, and N. Nagaosa, Nonlinear spin current generation in noncentrosymmetric spin-orbit coupled systems, Phys. Rev. B **95**, 224430 (2017).

[13] C. H. Lee, H. H. Yap, T. Tai, G. Xu, X. Zhang, and J. Gong, Enhanced higher harmonic generation from nodal topology, Phys. Rev. B **102**, 035138 (2020).

[14] Y. S. Ang, C. H. Lee, and L. K. Ang, Universal scaling and signatures of nodal structures in electron tunneling from two-dimensional semimetals, arXiv:2003.14004.

[15] C. Holzhey, F. Larsen, and F. Wilczek, Geometric and renormalized entropy in conformal field theory, Nucl. Phys. B **424**, 443 (1994).

[16] P. Calabrese and J. Cardy, Entanglement entropy and quantum field theory, J. Stat. Mech. (2004) P06002.

[17] M. M. Wolf, Violation of the Entropic Area Law for Fermions, Phys. Rev. Lett. **96**, 010404 (2006).

[18] S. Ryu and T. Takayanagi, Holographic Derivation of Entanglement Entropy from the Anti–De Sitter Space/Conformal Field Theory Correspondence, Phys. Rev. Lett. **96**, 181602 (2006).

[19] D. Gioev and I. Klich, Entanglement Entropy of Fermions in Any Dimension and the Widom Conjecture, Phys. Rev. Lett. **96**, 100503 (2006).

[20] T. Senthil, Critical Fermi surfaces and non-Fermi liquid metals, Phys. Rev. B **78**, 035103 (2008).

[21] S.-S. Lee, Stability of the U(1) spin liquid with a spinon Fermi surface in $2 + 1$ dimensions, Phys. Rev. B **78**, 085129 (2008).

[22] J. Eisert, M. Cramer, and M. B. Plenio, Colloquium: Area laws for the entanglement entropy, Rev. Mod. Phys. **82**, 277 (2010).

[23] B. Swingle, Entanglement Entropy and the Fermi Surface, Phys. Rev. Lett. **105**, 050502 (2010).

[24] X.-L. Qi, Exact holographic mapping and emergent spacetime geometry, arXiv:1309.6282.

[25] Y. Gu, C. H. Lee, X. Wen, G. Y. Cho, S. Ryu, and X.-L. Qi, Holographic duality between $(2+ 1)$-dimensional quantum anomalous Hall state and $(3+ 1)$-dimensional topological insulators, Phys. Rev. B **94**, 125107 (2016).

[26] Y.-Z. You, X.-L. Qi, and C. Xu, Entanglement holographic mapping of many-body localized system by spectrum bifurcation renormalization group, Phys. Rev. B **93**, 104205 (2016).

[27] Y. Xu, S.-T. Wang, and L.-M. Duan, Weyl Exceptional Rings in a Three-Dimensional Dissipative Cold Atomic Gas, Phys. Rev. Lett. **118**, 045701 (2017).

[28] K. Yamamoto, M. Nakagawa, K. Adachi, K. Takasan, M. Ueda, and N. Kawakami, Theory of Non-Hermitian Fermionic Superfluidity with a Complex-Valued Interaction, Phys. Rev. Lett. **123**, 123601 (2019).

[29] M. Papaj, H. Isobe, and L. Fu, Nodal arc of disordered Dirac fermions and non-Hermitian band theory, Phys. Rev. B **99**, 201107(R) (2019).

[30] H. Shen and L. Fu, Quantum Oscillation from In-Gap States and a Non-Hermitian Landau Level Problem, Phys. Rev. Lett. **121**, 026403 (2018).

[31] R. Hamazaki, K. Kawabata, and M. Ueda, Non-Hermitian Many-Body Localization, Phys. Rev. Lett. **123**, 090603 (2019).

[32] M. Nakagawa, N. Kawakami, and M. Ueda, Non-Hermitian Kondo Effect in Ultracold Alkaline-Earth Atoms, Phys. Rev. Lett. **121**, 203001 (2018).

[33] H. Zhao, X. Qiao, T. Wu, B. Midya, S. Longhi, and L. Feng, Non-Hermitian topological light steering, Science **365**, 1163 (2019).

[34] Z. Yang and J. Hu, Non-Hermitian Hopf-link exceptional line semimetals, Phys. Rev. B **99**, 081102(R) (2019).

[35] F. Song, S. Yao, and Z. Wang, Non-Hermitian Skin Effect and Chiral Damping in Open Quantum Systems, Phys. Rev. Lett. **123**, 170401 (2019).

[36] Y. Wu, W. Liu, J. Geng, X. Song, X. Ye, C.-K. Duan, X. Rong, and J. Du, Observation of parity-time symmetry breaking in a single-spin system, Science **364**, 878 (2019).

[37] L. Li, C. H. Lee, and J. Gong, Geometric characterization of non-Hermitian topological systems through the singularity ring in pseudospin vector space, Phys. Rev. B **100**, 075403 (2019).

[38] L. Zhou and J. Gong, Non-Hermitian floquet topological phases with arbitrarily many real-quasienergy edge states, Phys. Rev. B **98**, 205417 (2018).

[39] R. El-Ganainy, K. G. Makris, M. Khajavikhan, Z. H. Musslimani, S. Rotter, and D. N. Christodoulides, Non-Hermitian physics and PT symmetry, Nat. Phys. **14**, 11 (2018).

[40] Z. Gong, Y. Ashida, K. Kawabata, K. Takasan, S. Higashikawa, and M. Ueda, Topological Phases of Non-Hermitian Systems, Phys. Rev. X **8**, 031079 (2018).

[41] Q. Zhong, M. Khajavikhan, D. N. Christodoulides, and R. El-Ganainy, Winding around non-Hermitian singularities, Nat. Commun. **9**, 4808 (2018).

[42] T. Yoshida, R. Peters, and N. Kawakami, Non-Hermitian perspective of the band structure in heavy-fermion systems, Phys. Rev. B **98**, 035141 (2018).

[43] A. A. Zyuzin and A. Yu. Zyuzin, Flat band in disorder-driven non-Hermitian Weyl semimetals, Phys. Rev. B **97**, 041203(R) (2018).

[44] K. Kawabata, S. Higashikawa, Z. Gong, Y. Ashida, and M. Ueda, Topological unification of time-reversal and particle-hole symmetries in non-Hermitian physics, Nat. Commun. **10**, 297 (2019).

[45] K. Kawabata, T. Bessho, and M. Sato, Classification of Exceptional Points and Non-Hermitian Topological Semimetals, Phys. Rev. Lett. **123**, 066405 (2019).

[46] T. Yoshida, K. Kudo, and Y. Hatsugai, Non-Hermitian fractional quantum Hall states, Sci. Rep. **9**, 16895 (2019).

[47] C.-H. Liu and S. Chen, Topological classification of defects in non-Hermitian systems, Phys. Rev. B **100**, 144106 (2019).

[48] T. E. Lee, Anomalous Edge State in a Non-Hermitian Lattice, Phys. Rev. Lett. **116**, 133903 (2016).

[49] V. M. Martinez Alvarez, J. E. Barrios Vargas, and L. E. F. Foa Torres, Non-Hermitian robust edge states in one dimension: Anomalous localization and eigenspace condensation at exceptional points, Phys. Rev. B **97**, 121401(R) (2018).

[50] S. Yao and Z. Wang, Edge States and Topological Invariants of Non-Hermitian Systems, Phys. Rev. Lett. **121**, 086803 (2018).

[51] S. Yao, F. Song, and Z. Wang, Non-Hermitian Chern Bands, Phys. Rev. Lett. **121**, 136802 (2018).

[52] F. K. Kunst, E. Edvardsson, J. C. Budich, and E. J. Bergholtz, Biorthogonal Bulk-Boundary Correspondence in Non-Hermitian Systems, Phys. Rev. Lett. **121**, 026808 (2018).

[53] C. H. Lee and R. Thomale, Anatomy of skin modes and topology in non-Hermitian systems, Phys. Rev. B **99**, 201103(R) (2019).

[54] C. H. Lee, L. Li, and J. Gong, Hybrid Higher-Order Skin-Topological Modes in Nonreciprocal Systems, Phys. Rev. Lett. **123**, 016805 (2019).

[55] C. H. Lee, G. Li, Y. Liu, T. Tai, R. Thomale, and X. Zhang, Tidal surface states as fingerprints of non-Hermitian nodal knot metals, arXiv:1812.02011.

[56] K. Yokomizo and S. Murakami, Non-Bloch Band Theory of Non-Hermitian Systems, Phys. Rev. Lett. **123**, 066404 (2019).

[57] S. Longhi, Probing non-Hermitian skin effect and non-Bloch phase transitions, Phys. Rev. Research **1**, 023013 (2019).

[58] X. Zhang and J. Gong, Non-Hermitian Floquet topological phases: Exceptional points, coalescent edge modes, and the skin effect, Phys. Rev. B **101**, 045415 (2020).

[59] S. Longhi, Topological Phase Transition in Non-Hermitian Quasicrystals, Phys. Rev. Lett. **122**, 237601 (2019).

[60] C. H. Lee, L. Li, R. Thomale, and J. Gong, Unraveling non-Hermitian pumping: Emergent spectral singularities and anomalous responses, arXiv:1912.06974.

[61] H. Jiang, L.-J. Lang, C. Yang, S.-L. Zhu, and S. Chen, Interplay of non-Hermitian skin effects and Anderson localization in nonreciprocal quasiperiodic lattices, Phys. Rev. B **100**, 054301 (2019).

[62] C. H. Lee, Many-body topological and skin states without open boundaries, arXiv:2006.01182.

[63] T. Yoshida, R. Peters, N. Kawakami, and Y. Hatsugai, Symmetry-protected exceptional rings in two-dimensional correlated systems with chiral symmetry, Phys. Rev. B **99**, 121101(R) (2019).

[64] W. Zheng and N. R. Cooper, Superradiance Induced Particle Flow Via Dynamical Gauge Coupling, Phys. Rev. Lett. **117**, 175302 (2016).

[65] A. Ghatak, M. Brandenbourger, J. van Wezel, and C. Coulais, Observation of non-Hermitian topology and its bulk-edge correspondence, arXiv:1907.11619.

[66] T. Helbig, T. Hofmann, S. Imhof, M. Abdelghany, T. Kiessling, L. W. Molenkamp, C. H. Lee, A. Szameit, M. Greiter, and R. Thomale, Generalized bulk–boundary correspondence in non-Hermitian topolectrical circuits, Nat. Phys. **16**, 747 (2020).

[67] L. Xiao, T. Deng, K. Wang, G. Zhu, Z. Wang, W. Yi, and P. Xue, Observation of non-Hermitian bulk-boundary correspondence in quantum dynamics, Nat. Phys. **16**, 761 (2020).

[68] T. Hofmann, T. Helbig, F. Schindler, N. Salgo, M. Brzezińska, M. Greiter, T. Kiessling, D. Wolf, A. Vollhardt, A. Kabaši *et al.*, Reciprocal skin effect and its realization in a topolectrical circuit, Phys. Rev. Research **2**, 023265 (2020).

[69] X. Z. Zhang and Z. Song, Momentum-independent reflectionless transmission in the non-Hermitian time-reversal symmetric system, Ann. Phys. **339**, 109 (2013).

[70] A. R. Its, B.-Q. Jin, and V. E. Korepin, Entanglement in the *XY* spin chain, J. Phys. A: Math. Gen. **38**, 2975 (2005).

[71] A. R. Its and V. E. Korepin, The Fisher-Hartwig formula and entanglement entropy, J. Stat. Phys. **137**, 1014 (2009).

[72] C. H. Lee, P. Ye, and X.-L. Qi, Position-momentum duality in the entanglement spectrum of free fermions, J. Stat. Mech. (2014) P10023.

[73] See Supplemental Material at http://link.aps.org/supplemental/10.1103/PhysRevB.102.081115 for details on analytic derivations for the spatial density distribution, entanglement entropy computations, and PBC-OBC spectral interpolation, which includes Refs. [16,53,72,74,94–100].

[74] P. Calabrese and J. Cardy, Entanglement entropy and conformal field theory, J. Phys. A: Math. Theor. **42**, 504005 (2009).

[75] Loïc Herviou, N. Regnault, and J. H. Bardarson, Entanglement spectrum and symmetries in non-Hermitian fermionic non-interacting models, SciPost Phys. **7**, 069 (2019).

[76] P.-Y. Chang, J.-S. You, X. Wen, and S. Ryu, Entanglement spectrum and entropy in topological non-Hermitian systems and non-unitary conformal field theories, Phys. Rev. Research **2**, 033069 (2020).

[77] Note that for large β outside Region 1 in Fig. 2(a), the oscillation of the EE is a consequence of the interplay between the oscillatory nature of the ground state and the asymmetric pumping [73].

[78] This definition is identical to that in Hermitian cases, but alternative biorthogonal or SVD definitions exist [75].

[79] L. Li, C. H. Lee, and J. Gong, Topological Switch for Non-Hermitian Skin Effect in Cold-Atom Systems with Loss, Phys. Rev. Lett. **124**, 250402 (2020).

[80] M. A. Cazalilla, R. Citro, T. Giamarchi, E. Orignac, and M. Rigol, One dimensional bosons: From condensed matter systems to ultracold gases, Rev. Mod. Phys. **83**, 1405 (2011).

[81] X.-W. Guan, M. T. Batchelor, and C. Lee, Fermi gases in one dimension: From Bethe ansatz to experiments, Rev. Mod. Phys. **85**, 1633 (2013).

[82] J. H. Kang, J. H. Han, and Y. il Shin, Topological Creutz ladder in a resonantly shaken 1D optical lattice, New J. Phys. **22**, 013023 (2020).

[83] Y. Ashida, S. Furukawa, and M. Ueda, Quantum critical behavior influenced by measurement backaction in ultracold gases, Phys. Rev. A **94**, 053615 (2016).

[84] Y. Ashida and M. Ueda, Full-Counting Many-Particle Dynamics: Nonlocal and Chiral Propagation of Correlations, Phys. Rev. Lett. **120**, 185301 (2018).

[85] Y. Ashida, *Quantum Many-Body Physics in Open Systems: Measurement and Strong Correlations* (Springer Nature, London, 2020).

[86] Y. Ashida, S. Furukawa, and M. Ueda, Parity-time-symmetric quantum critical phenomena, Nat. Commun. **8**, 15791 (2017).

[87] S. Lapp, J. Ang'ong'a, F. Alex An, and B. Gadway, Engineering tunable local loss in a synthetic lattice of momentum states, New J. Phys. **21**, 045006 (2019).

[88] J. Li, A. K. Harter, J. Liu, L. de Melo, Y. N. Joglekar, and L. Luo, Observation of parity-time symmetry breaking transitions in a dissipative Floquet system of ultracold atoms, Nat. Commun. **10**, 855 (2019).

[89] P. Würtz, T. Langen, T. Gericke, A. Koglbauer, and H. Ott, Experimental Demonstration of Single-Site Addressability in a Two-Dimensional Optical Lattice, Phys. Rev. Lett. **103**, 080404 (2009).

[90] C. Kollath, M. Köhl, and T. Giamarchi, Scanning tunneling microscopy for ultracold atoms, Phys. Rev. A **76**, 063602 (2007).

[91] T. Gericke, P. Würtz, D. Reitz, T. Langen, and H. Ott, High-resolution scanning electron microscopy of an ultracold quantum gas, Nat. Phys. **4**, 949 (2008).

[92] P. Weinberg and M. Bukov, QuSpin: A Python package for dynamics and exact diagonalisation of quantum many body systems. Part I: Spin chains, SciPost Phys. **2**, 003 (2017).

[93] P. Weinberg and M. Bukov, QuSpin: A Python Package for dynamics and exact diagonalisation of quantum many body systems. Part II: Bosons, fermions and higher spins, SciPost Phys. **7**, 20 (2019).

[94] L. He and D. Vanderbilt, Exponential Decay Properties of Wannier Functions and Related Quantities, Phys. Rev. Lett. **86**, 5341 (2001).

[95] I. Peschel and V. Eisler, Reduced density matrices and entanglement entropy in free lattice models, J. Phys. A: Math. Theor. **42**, 504003 (2009).

[96] A. Alexandradinata, T. L. Hughes, and B. Andrei Bernevig, Trace index and spectral flow in the entanglement spectrum of topological insulators, Phys. Rev. B **84**, 195103 (2011).

[97] H. Matsueda, Holographic entanglement entropy in Suzuki-Trotter decomposition of spin systems, Phys. Rev. E **85**, 031101 (2012).

[98] C. H. Lee, Y. Yamada, T. Kumamoto, and H. Matsueda, Exact mapping from singular-value spectrum of fractal images to entanglement spectrum of one-dimensional quantum systems, J. Phys. Soc. Jpn. **84**, 013001 (2014).

[99] C. H. Lee and P. Ye, Free-fermion entanglement spectrum through Wannier interpolation, Phys. Rev. B **91**, 085119 (2015).

[100] C. H. Lee, D. P. Arovas, and R. Thomale, Band flatness optimization through complex analysis, Phys. Rev. B **93**, 155155 (2016).